Proceedings of the Seventh International Conference on
Railway Technology: Research, Development and Maintenance
Edited by: J. Pombo
Civil-Comp Conferences, Volume 15, Paper 10.3
Civil-Comp Press, Edinburgh, United Kingdom, 2026
ISSN: 2753-3239, doi: 10.4203/ccc.15.10.3

A Validated Methodology for Assessing Wind-Induced Effects on Pantograph-Catenary Interaction

J. M. Rebelo[1], J. Pombo[1,2,3], P. Antunes[1,2], J. Santos[1], F. Jackson[1], P. Schito[4], A. Facchinetti[4], D. Campbell[5], R. Stainton[5] and M. Askill[6]

[1]**Institute of Railway Research, University of Huddersfield, United Kingdom**
[2]**IDMEC, Instituto Superior Técnico, Universidade de Lisboa, Lisbon, Portugal**
[3]**ISEL, Instituto Politecnico de Lisboa, Lisbon, Portugal**
[4]**Department of Mechanical Engineering, Politecnico di Milano, Italy**
[5]**Network Rail, United Kingdom**
[6]**Wabtec, United Kingdom**

Abstract

This paper presents a comprehensive assessment of the aerodynamic behaviour of the HSP pantograph using full-scale wind-tunnel testing, Computational Fluid Dynamics (CFD) and pantograph-overhead line equipment (OLE) dynamic simulations. Wind-tunnel tests are conducted across a range of pantograph heights, wind speeds and yaw angles to quantify aerodynamic forces, moments and uplift. Results show that aerodynamic uplift is highly sensitive to pantograph extension, wind speed and flow direction, with increasing variability at higher speeds.

A CFD framework is developed and validated against the experimental data, demonstrating good agreement with measured aerodynamic loads. The validated model is subsequently applied to conditions beyond the wind-tunnel envelope, including high-speed headwinds and multiple-pantograph operations. Simulations revealed significant aerodynamic interference effects between pantographs, influenced by spacing, roof-flow development, knuckle orientation and vane angles.

The CFD aerodynamic loads are incorporated into pantograph-OLE dynamic simulations. The results show that aerodynamic loading influences contact force magnitude and variability, affecting current collection performance, while generally remaining within acceptance limits. The methodology presented here provides a robust basis for assessing wind-induced pantograph behaviour and supports improved modelling, operational practice and future standards development.

Keywords: pantograph-catenary interaction, current collection performance, contact forces, computational fluid dynamics, aerodynamic forces, 3D finite element model.

1. Introduction

This work investigates the aerodynamic performance of a full-scale Wabtec/Brecknell Willis HSP pantograph under a wide range of operating and environmental conditions. While standards such as EN50317 [1] and EN50318 [2] define methods for assessing pantograph-catenary interaction and validating simulation tools, they do not explicitly consider the effects of crosswinds, varying contact wire heights, or multi-pantograph operations. To address these gaps, a programme of full-scale wind tunnel testing and high-fidelity CFD analysis is undertaken, quantifying pantograph drag and uplift across different wind speeds, wind directions, train speeds, pantograph heights, and multi-pantograph configurations.

The experimental and numerical studies are setup similarly as to enable direct comparison of results and the development of reliable aerodynamic force models. The resulting dataset improves understanding of how aerodynamic loads affect pantograph behaviour and OLE interaction. These validated models are incorporated into dynamic pantograph-catenary simulations to assess impact on current collection performance. The study provides a comprehensive assessment of wind-induced effects and supports future modelling, design improvements and potential updates to industry standards.

2. Full-Scale Wind Tunnel Testing

The aerodynamic tests of the HSP pantograph are conducted at the POLIMI full-scale wind tunnel facility, detailed in Figure 1. It is a vertical closed-circuit wind tunnel featuring two test sections, enabling a wide range of flow conditions. The pantograph tests are performed in the high-speed, low-turbulence test section, located in the lower leg of the loop. This 6-m long chamber has a cross-section of approximately 4 m × 4 m and a maximum wind speed of 55 m/s, with a turbulence intensity below 0.15%. The test section is equipped with a 2.5 m diameter turntable and adjustable supports to vary the perceived flow angle.

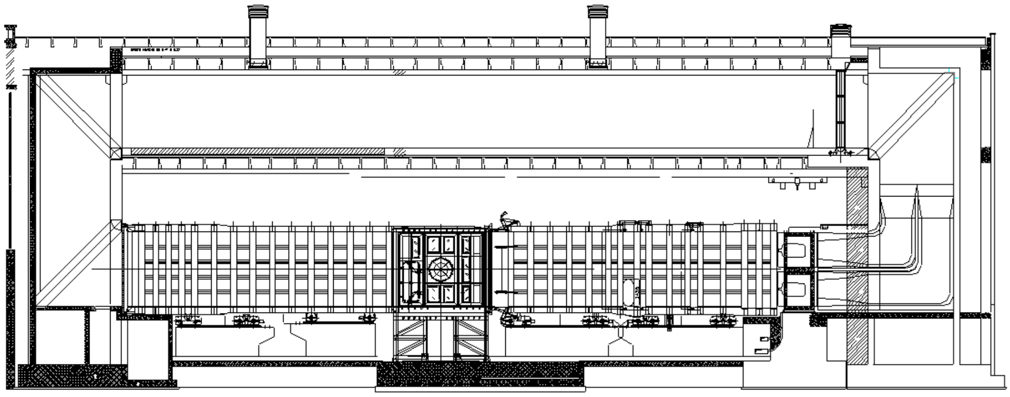

Figure 1: Longitudinal section of the POLIMI wind tunnel.

The dimensions of the high-speed section enable testing of the pantograph at full-scale with negligible blockage effects, removing the need for geometric scaling and associated Reynolds number corrections. The test setup is specifically designed to rigidly mount the pantograph onto a supporting frame, itself connected to a six-component dynamometric balance anchored to the ground, as shown in Figure 2. This allows for the direct measurement of the total aerodynamic loads acting on the pantograph. The forces and moments along the three main axes are recorded as a function of wind speed. Additionally, load cells are installed on the pantograph base and connected to the head via tethers, providing measurements of the aerodynamic lift acting directly on the pantograph collector strips. This is the most relevant parameter for the analysis of pantograph-catenary interaction and current collection performance.

Figure 2: Pantograph setup at wind tunnel.

The pantograph is tested at three vertical configurations, corresponding to different effective contact wire heights. Measured from splitter plate/pantograph base, they correspond to:

- *H1*: Minimum height (695 mm).
- *H2*: Nominal height: (1202 mm).
- *H3*: Maximum height: (2290 mm).

For each height configuration, wind direction sensitivity is assessed by rotating the pantograph relative to the incoming flow. This is expressed as a yaw angle (*a*), where *a* = 0º and *a* = 180º correspond to knuckle trailing and knuckle leading configurations respectively. The angles considered vary between the two knuckle configurations in 10º increments.

Tests are conducted across a wide range of speeds up to the operational limits of the test facility, from 20 to 50 m/s (45 to 112 mph), in 5 m/s (11.25mph) increments.

The full-scale wind tunnel test results of HSP pantograph demonstrate that:

- The pantograph aerodynamic uplift is strongly dependent on the operating height, with higher configurations producing increased mean lift and variability.
- Wind direction induces significant asymmetry in loading, particularly under oblique cross wind conditions.
- Lift variability increases with wind speed, indicating a potential contribution to contact force fluctuations during operation.

These findings provide quantitative evidence supporting the inclusion of height and direction dependent aerodynamic loading in pantograph dynamic models, enabling improved prediction of current collection quality under adverse aerodynamic conditions, beyond the capabilities of traditional tethered or static testing alone.

3. CFD Studies of the HSP Pantograph

Computational Fluid Dynamics (CFD) is used to assess the aerodynamic performance of the HSP pantograph and extend wind-tunnel results to realistic operating conditions. The approach relies on a validated numerical framework, with CFD predictions first benchmarked against wind-tunnel measurements covering different pantograph heights, orientations and flow speeds. This validation is essential given the complex geometry of the pantograph and its effect on flow behaviour.

The CFD study has four objectives: (1) reproduce wind-tunnel aerodynamic forces accurately, (2) develop an efficient yet realistic geometric model, (3) provide detailed flow-field information such as pressure, velocity and turbulence distributions, and (4) analyse double- and triple-pantograph configurations. Simulations investigate conditions beyond the wind-tunnel range, including combined train speed and headwind effects, interactions between multiple pantographs, and roof boundary-layer development.

The CFD pantograph model is developed from CAD geometry and modified to better match the wind-tunnel test configuration, particularly around the base region where geometric differences can influence aerodynamic forces and flow separation. A defeaturing strategy, depicted in Figure 3, removing minor details while retaining key structural components such as the head, vanes, upper and lower arms, base frame and supports. This approach reduces computational cost while preserving the main aerodynamic characteristics, ensuring reliable comparison with experimental results and reliable prediction of global aerodynamic loads. Furthermore, the decomposition into individual components, presented in Figure 4, enables the interpretation of aerodynamic forces at component level rather than only at full-assembly level.

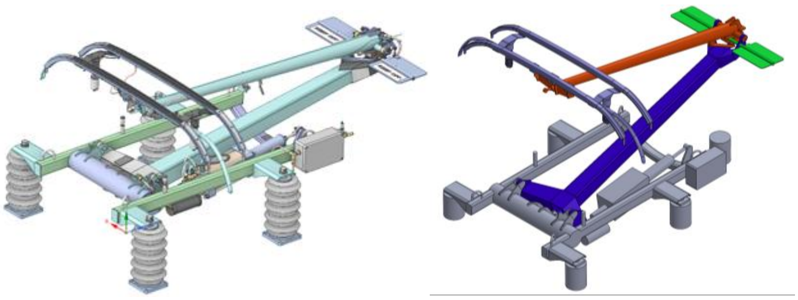

Figure 3: Original and defeatured pantograph CAD models.

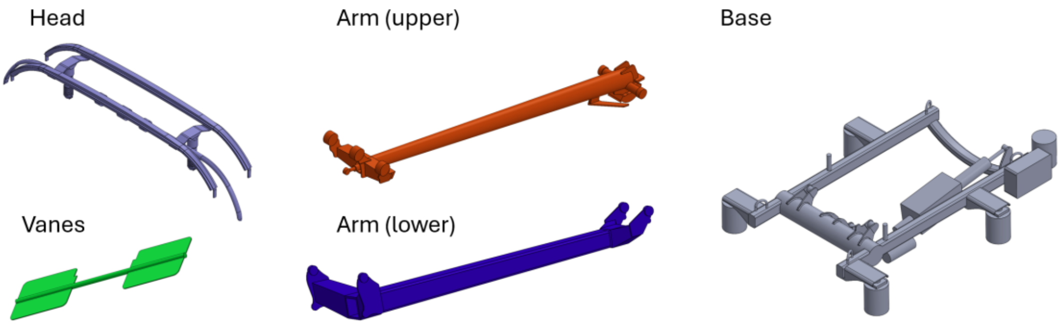

Figure 4: Pantograph CAD model components.

The CFD domain is designed to replicate the wind-tunnel test section, using a 4 m × 4 m cross-section with the pantograph positioned 7 m from the inlet and 15 m from the outlet. These distances minimise inlet effects and allow for adequate wake development, including vortex shedding, turbulence evolution and pressure recovery. Boundary conditions consist of a uniform velocity inlet, a zero-gauge pressure outlet, and no-slip walls on the ground, sides and roof to capture wind-tunnel blockage effects. Convergence is assessed by monitoring force, moment and residuals.

Mesh development is refined iteratively to achieve agreement with experimental lift, drag and moment data. Local refinements are applied to critical regions such as the head, arms, vanes and base, as depicted in Figure 5.

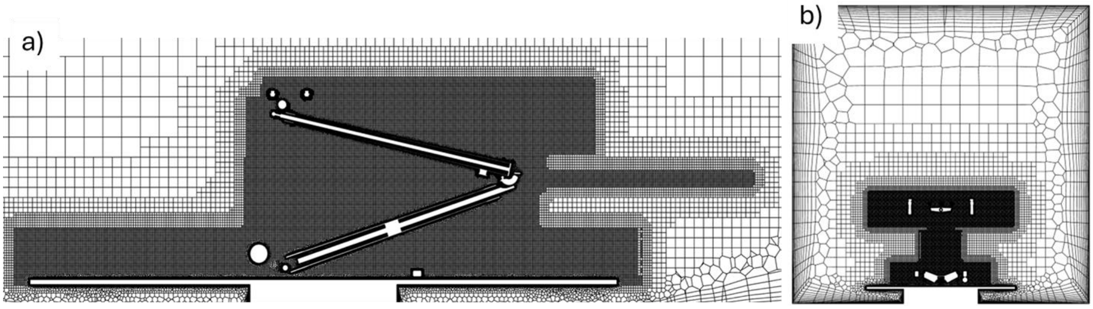

Figure 5: CFD mesh with refinement zones; a) Side view, b) Front view

The CFD model is validated against wind-tunnel measurements across a range of flow speeds and pantograph heights, focusing on the prediction of global aerodynamic loads, including drag, lift and moment. During the simulations, force and moment values initially showed significant fluctuations before stabilising as the solution converged. The introduction of a pseudo-transient solver after 2000 iterations improved residual convergence and reduced oscillations, allowing mean values to be calculated from the stable portion of the solution. The evolution of lift force for each component is presented in Figure 6.

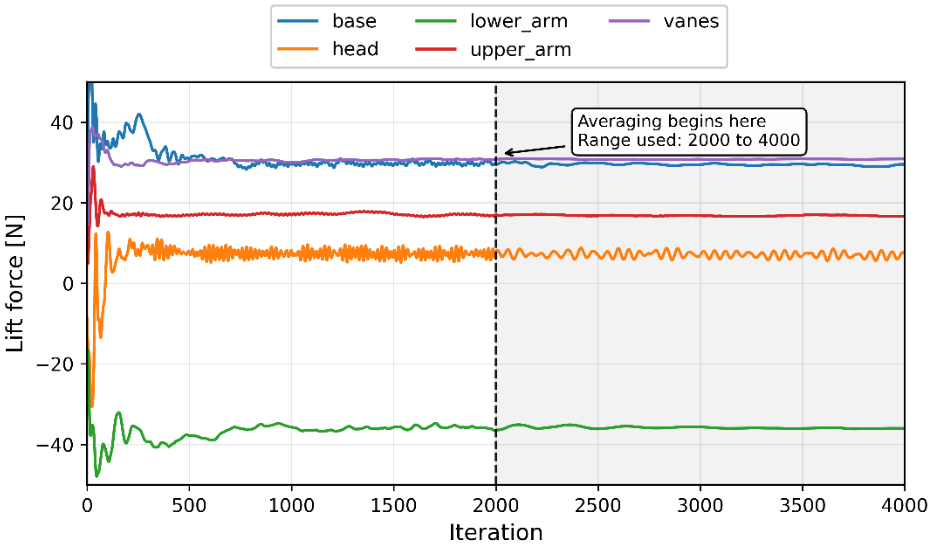

Figure 6: CFD lift forces per component.

Comparison with wind-tunnel results, in Table 1, demonstrates generally strong agreement, confirming the reliability of the CFD model. Discrepancies between numerical and experimental data only exceed 15% only for the H3 pantograph configuration at the higher flow speeds of 30 and 40 m/s, and only in drag-force predictions. This overall agreement provides confidence in the CFD framework for further analysis.

Speed [m/s]	Parameter	Height H1			Height H2			Height H3		
		WT [N], [Nm]	CFD [N], [Nm]	Deviation [%]	WT [N], [Nm]	CFD [N], [Nm]	Deviation [%]	WT [N], [Nm]	CFD [N], [Nm]	Deviation [%]
20	Drag	113.6	109.7	-3.5%	119.0	110.3	-7.3%	120.3	123.6	2.8%
	Lift	18.0	18.0	0.2%	20.5	19.7	-4.0%	20.5	21.9	7.1%
	Moment	34.4	33.1	-3.9%	59.8	56.4	-5.7%	124.8	115.0	-7.9%
30	Drag	251.7	245.7	-2.4%	262.4	244.5	-6.8%	330.6	274.2	-17.1%
	Lift	39.8	40.6	2.0%	45.1	46.5	3.1%	55.6	48.5	-12.9%
	Moment	76.1	75.2	-1.1%	131.3	124.9	-4.9%	283.6	255.5	-9.9%
40	Drag	439.2	435.8	-0.8%	459.8	435.4	-5.3%	578.8	489.2	-15.5%
	Lift	70.3	71.5	1.8%	77.5	77.6	0.2%	91.6	85.2	-7.0%
	Moment	133.2	133.9	0.6%	225.1	221.2	-1.7%	492.7	456.4	-7.4%

Table 1: Comparison of CFD and Wind Tunnel (WT) results.

A further objective of the CFD study is to investigate operating conditions beyond those examined in the wind-tunnel programme. One such scenario considers the H2 pantograph configuration at a train speed of 125 mph and under a 25 m/s (55 mph) headwind, resulting in an effective flow speed of 80.5 m/s (180 mph, 290 km/h). The simulations show that these combined operating conditions significantly increase the aerodynamic loads on the pantograph. Furthermore, the evolution of these forces along train speed follows a nearly quadratic regression, as depicted in Figure 7, and closely matching the aerodynamic uplift force component defined in EN 50367 [3].

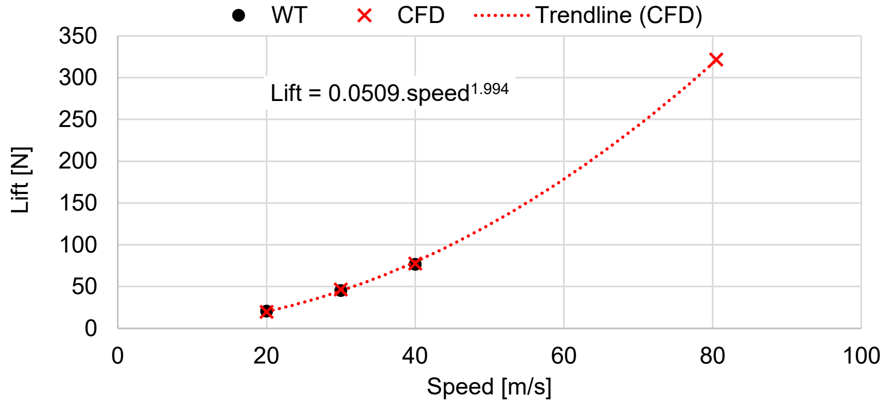

Figure 7: CFD lift forces at height H2 and various speeds.

To investigate the aerodynamic behaviour of the HSP pantograph in multiple-pantograph operation, a CFD model of the Aventra train and pantograph system is developed. The computational domain is scaled to the train height, with sufficient clearances in all directions to capture the development of the flow and pantograph wakes.

The computational mesh combines a structured background mesh with local refinements around the train body, roof equipment and pantographs. Fine mesh resolution was applied to pantograph components and near-wall regions to accurately capture flow separation, vortex formation, wake development and other complex aerodynamic phenomena, while coarser cells were used farther from the train to improve computational efficiency. The different levels of mesh refinement are presented in Figure 8. Simulations follow the setup used in the validated wind-tunnel studies, although with increased number of iterations from 4000 to 8000 due to the greater flow complexity.

Three scenarios are selected: double pantograph operation with 121 and 193 m spacing, and triple pantograph with 73/89 m spacings, the latter presented in Figure 9. All simulations consider a train speed of 125 mph (55 m/s).

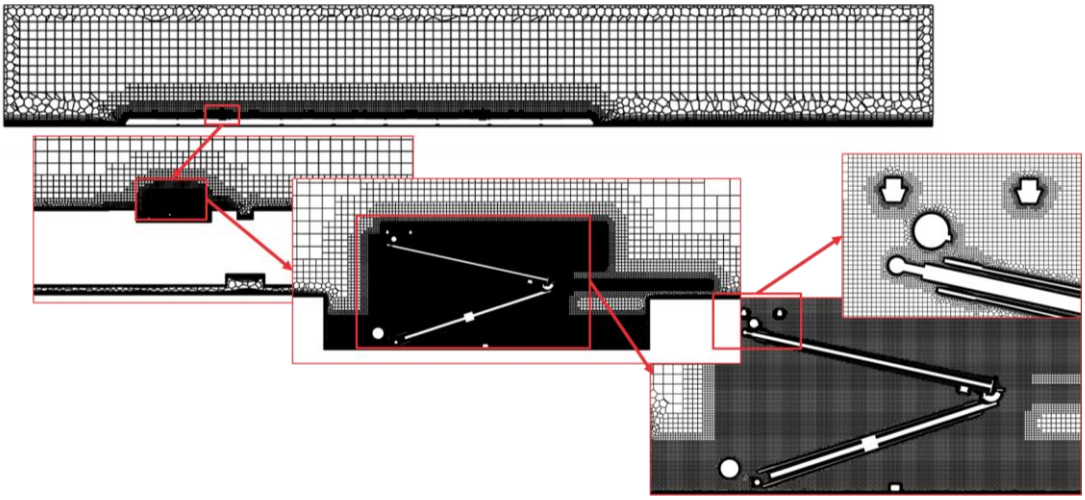

Figure 8: Side view of train and pantograph CFD mesh with refinement areas.

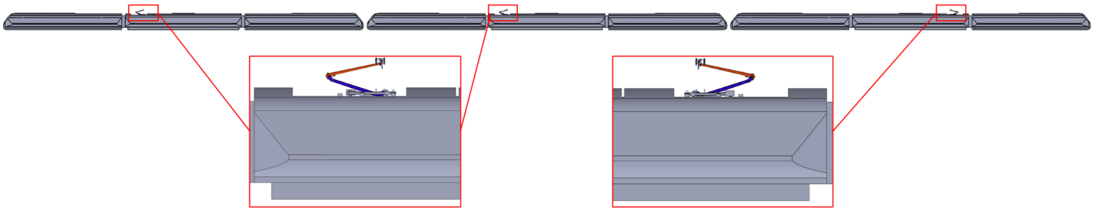

Figure 9: Triple pantograph configuration with 73 m and 89 m spacing.

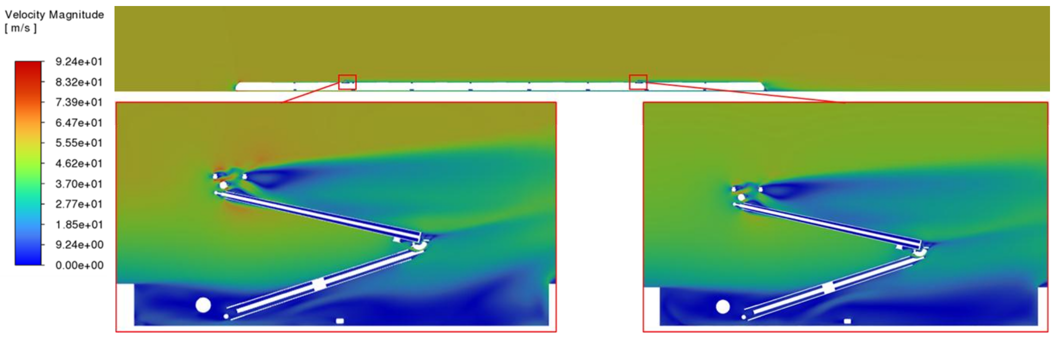

Figure 10: Velocity field of double pantograph configuration with 121 m spacing.

The virtual work principle is used to compute the resulting pantograph aerodynamic uplift on the contact wire from the loads obtained via CFD. The uplifts are summarised in Table 2. In multi-pantograph operation, wake interactions and flow distortion from upstream pantographs strongly influence the loads experienced by downstream units. Double-pantograph configurations generally lead to lower aerodynamic loads on the trailing pantograph, while in triple-pantograph operation, knuckle orientation and vane-angle considerably influence the resulting uplift. Overall, aerodynamic uplift depends not only on train speed but also on roof-flow development, pantograph extension, location along train and interference effects from other units, highlighting the need to account for these factors in pantograph-catenary dynamic analyses.

Speed	Configuration	Height	Panto F_A [N]		
			First	Second	Third
125 mph 55.5 m/s	Triple 73/89 m KL/KL/KT	H1	-2.2	-6.8	22.5
		H2	-25.5	-20.6	35.0
		H3	-40.2	-32.4	58.5
	Double 121 m KT/KT	H1	13.9	13.1	n.a.
		H2	52.9	39.5	
		H3	73.6	61.7	
	Double 193 m KT/KT	H1	30.1	22.0	
		H2	42.3	30.9	
		H3	69.5	57.8	

Table 2: Uplift forces for multiple pantograph configurations.

4. Pantograph-OLE Interaction with Realistic Aerodynamic Loads

The aerodynamic uplift loads on pantographs are integrated into realistic pantograph-OLE (overhead line equipment) dynamic interaction studies using *PantoCat* software [4–8]. The aim is to assess how these wind-induced loads affect the contact forces and the current collection quality [9,10].

The OLE system UKMS125 [11] is considered in this work, which allows for train speeds up to 125 mph. The numerical model is built using a 3D finite element formulation. The properties of the OLE components and the geometric description are summarised in Table 3. The catenary damping is achieved by using a structural damping matrix, as described in EN 50318 section A.2.1 [12].

Component	Material	Area [mm^2]	Tension [N]
Contact Wire (CW)	CuAg	120	15000
Messenger Wire (MW)	CuMg (stranded)	66	12000
Droppers (DRP)	CuMg (stranded)	10	n.a.
Steady Arm (SA)	Al	260	n.a.

Parameter	Value
Span Length [m]	50
Steady Arm Length [m]	1.10
Stagger [m]	0.23
CW height (nominal) [m]	4.70
System Height [m]	1.30

Table 3: UKMS125 properties and geometry

The finite element mesh of the OLE model is presented in Figure 11 to Figure 13. They depict, respectively, a side view of the entire model, and side and top views of the overlap. Figure 12 also includes a legend with the colour coding of the different OLE wires and components. Please note the difference in scaling between the vertical and horizontal axes. The area of interest includes 10 standard spans, followed by the 3-span overlap, and another 10 standard spans. The area shaded in grey in the Figure 11 is not part of the area of interest. The pantograph starting positions are within the left greyed area and at least 300 m before the actual area of interest, thus ensuring transient effects do not influence the dynamic results.

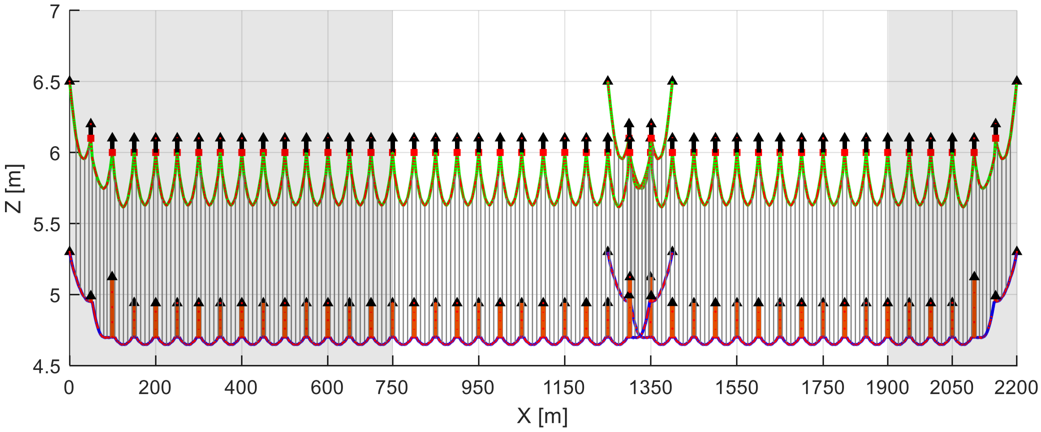

Figure 11: Finite element mesh of the OLE model: Side view

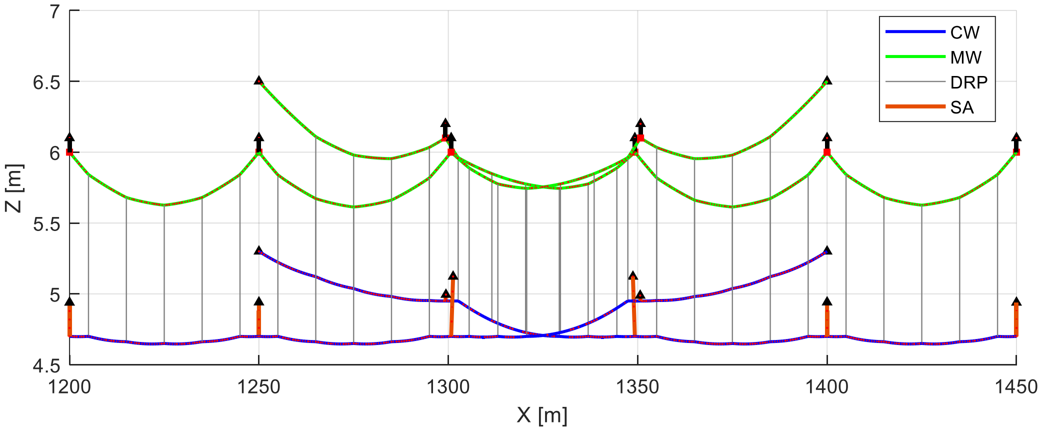

Figure 12: Finite element mesh of the OLE model: Overlap side view

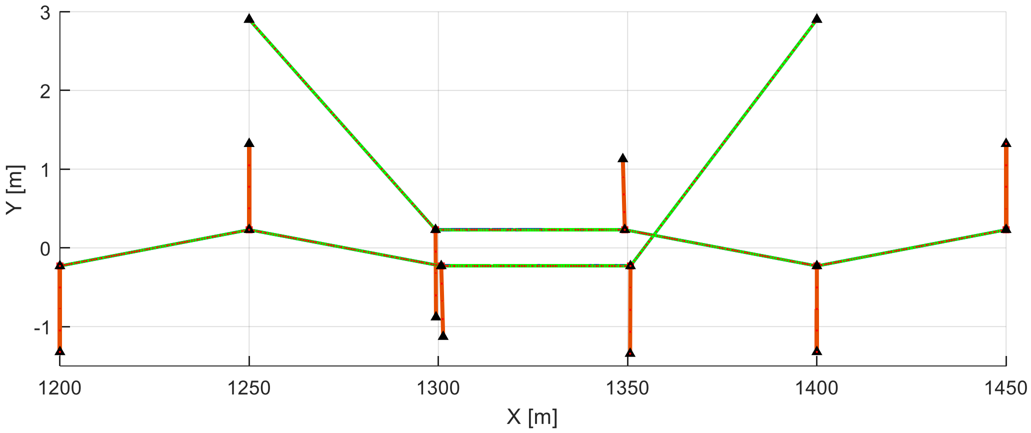

Figure 13: Finite element mesh of the OLE model: Overlap top view

The Wabtec/Brecknell Willis HSP Mk2 pantograph considered in this study is modelled as a linear three-stage lumped-mass system, with springs and dampers. The parameters of the model are determined experimentally [13,14] and are presented in Figure 14. Here, F_S represents the static uplift force (set to 90 N for all pantographs) F_A the aerodynamic uplift force, and F_C is the contact force that results from the dynamic interaction of the pantograph with the overhead system.

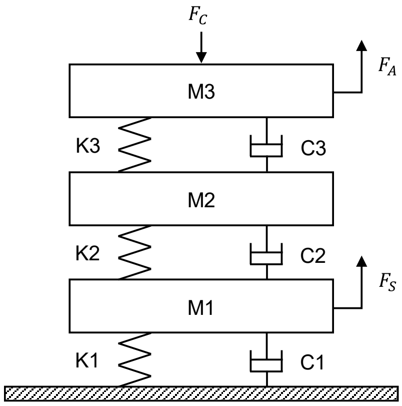

Parameter	Units	Value
M3	kg	5.14
M2		7.50
M1		3.53
K3	N/m	5700
K2		7000
K1		0
C3	Ns/m	110
C2		0
C1		32.6

Figure 14: HSP Mk2 pantograph lumped-mass model

Four aerodynamic scenarios are considered here. The baseline (*BSL*) uses the assumption given in EN 50367 table 6 [3], in which the uplift force is a function of the square of the train speed, as described in Table 4. The static force on the equation also changes depending on whether the train speed is below or above 200 kph (125 mph). Otherwise, both F_S and F_A are the same regardless of which pantograph is considered (leading or trailing), location within the train, spacing, working extension or knuckle orientation. The remaining three aerodynamic scenarios correspond to the three pantograph heights (*H1*, *H2* and *H3*) that have been analysed via CFD and presented in Table 2.

$v \leq 200$ km/h	$v > 200$ km/h
$0{,}000\,47\ v^2 + 90$	$0{,}000\,97\ v^2 + 70$

Table 4: EN 50367 pantograph uplift force setup

The pantograph-OLE interaction is assessed via statistical analysis of the contact force and support uplift. The forces are low-pass filtered with a cut-off frequency of 20 Hz, as per EN 50317 [1]. Contact quality is assessed according to the performance criteria detailed in Table 5.

Criterion	Standard	Parameter	Threshold
Maximum Contact Force	EN 50119:2020	Max	≤ 300 N
Minimum Statistical Minimum		St Min	> 0 N
Maximum Standard Deviation	EN 50367:2020+A2:2025	SD/Mean	≤ 0.3
Maximum Uplift at Support		Max Up	≤ 125 mm *

Table 5: Performance criteria for pantograph-OLE interaction

The dynamic assessment results at 125 mph are presented in Table 7. The shaded cells represent the values that exceed the allowed thresholds. Results show that the aerodynamic uplift has a significant influence on pantograph-OLE interaction. When the CFD-derived aerodynamic uplift forces are applied to the pantograph model, the simulations reveal increased maximum and mean contact forces and greater force variability (standard deviation), when compared to the baseline EN 50367 uplift formulation.

In the baseline triple pantograph scenario, the current collection performance of the trailing pantograph fails to meet the requirements defined in the standards in terms of *SD/Mean* ratio. When considering the CFD aerodynamic values, the increased uplift leads to both lower standard deviation and higher mean contact force, thus bringing the ratio within the threshold.

Across all scenarios, the results indicate that wind-induced forces can noticeably affect current collection quality. Higher uplift tends to push the pantograph closer to the upper limits of acceptable contact forces, increasing the risk of excessive mechanical wear. Downward forces raise the *SD/Mean* ratio and the likelihood of loss-of-contact events that can cause arcing and, consequently, electrical wear. Therefore, these findings demonstrate that aerodynamic effects cannot be neglected in high-speed operation and that validated, height-, orientation- and wind-dependent aerodynamic models, such as those developed in this study, are important for realistic pantograph-catenary dynamic performance assessment.

Panto Config	Aero Setup	Aero Force [N]	Panto	Filtered Contact Force [0 - 20 Hz]								Max Up [mm]
				Max [N]	Min [N]	A [N]	Mean [N]	SD [N]	SD/ Mean	St Max [N]	St Min [N]	
Thresholds				≤ 300.0	-	-	-	-	≤ 0.300	-	> 0.0	≤ 125
Double 121 m KT/KT	BSL	18.8	P1	162.0	58.1	103.9	108.8	19.9	0.183	168.6	49.0	65.9
		18.8	P2	164.5	49.1	115.4	108.8	21.3	0.196	172.7	44.9	
	CFD H1	36.2	P1	176.7	74.1	102.6	126.2	20.5	0.163	187.7	64.6	78.9
		26.1	P2	182.4	48.7	133.8	116.1	24.0	0.207	188.1	44.1	
	CFD H2	22.9	P1	167.4	61.8	105.6	112.8	20.1	0.178	173.2	52.5	68.9
		16.2	P2	163.4	44.8	118.7	106.2	21.6	0.204	171.1	41.2	
	CFD H3	31.1	P1	173.5	70.0	103.5	121.1	20.2	0.167	181.6	60.6	75.1
		29.1	P2	183.4	52.7	130.7	119.1	23.6	0.198	189.9	48.2	
Double 193 m KT/KT	BSL	18.8	P1	162.6	49.8	112.7	108.8	22.5	0.207	176.4	41.2	65.4
		18.8	P2	188.7	23.8	164.9	108.8	24.8	0.228	183.1	34.5	
	CFD H1	25.0	P1	168.4	55.1	113.3	115.0	22.8	0.198	183.5	46.6	70.0
		18.0	P2	190.0	20.8	169.3	107.9	25.2	0.233	183.5	32.4	
	CFD H2	25.6	P1	169.0	55.6	113.4	115.7	22.9	0.198	184.2	47.1	70.5
		18.1	P2	190.4	20.8	169.6	108.0	25.2	0.233	183.7	32.4	
	CFD H3	22.9	P1	167.2	52.5	114.8	112.9	22.8	0.202	181.4	44.4	68.5
		23.4	P2	194.8	27.6	167.1	113.3	24.8	0.218	187.6	39.1	

Table 6: Dynamic results at 125 mph, double pantograph configurations.

Panto Config	Aero Setup	Aero Force [N]	Panto	Filtered Contact Force [0 - 20 Hz]								Max Up [mm]
				Max [N]	Min [N]	A [N]	Mean [N]	SD [N]	SD/ Mean	St Max [N]	St Min [N]	
Thresholds				≤ 300.0	-	-	-	-	≤ 0.300	-	> 0.0	≤ 125
Triple 73/89 m KL/KL/KT	BSL	18.8	P1	162.8	61.3	101.5	108.8	19.6	0.180	167.5	50.1	86.4
		18.8	P2	159.3	55.2	104.1	108.8	18.5	0.170	164.4	53.2	
		18.8	P3	193.8	0.0	197.6	108.8	33.4	0.307	208.9	8.7	
	CFD H1	2.2	P1	141.8	45.9	95.9	92.1	19.0	0.206	149.2	35.1	82.6
		-3.5	P2	136.0	33.9	102.1	86.6	18.2	0.210	141.1	32.1	
		18.8	P3	185.4	0.0	185.7	108.8	30.0	0.276	198.9	18.6	
	CFD H2	-17.1	P1	127.9	28.2	99.7	72.8	19.8	0.272	132.3	13.4	81.2
		-15.3	P2	135.2	22.1	113.1	74.8	19.9	0.266	134.5	15.0	
		21.1	P3	181.5	11.3	170.2	111.0	27.4	0.246	193.1	29.0	
	CFD H3	-10.5	P1	132.6	34.2	98.4	79.5	19.4	0.244	137.7	21.2	82.3
		-8.4	P2	137.4	29.4	108.1	81.6	19.0	0.232	138.5	24.7	
		20.9	P3	183.5	7.2	176.3	110.9	28.3	0.255	195.6	26.1	

Table 7: Dynamic results at 125 mph, triple pantograph configuration.

5. Conclusions and Contributions

This work combines full-scale wind-tunnel testing, CFD modelling and pantograph-OLE dynamic simulations to comprehensively assess the aerodynamic behaviour of the HSP pantograph. Wind-tunnel measurements quantify the effects of pantograph height, wind speed and yaw angle on aerodynamic forces, moments and uplift, showing that uplift is highly sensitive to operating conditions.

A validated CFD framework accurately reproduces experimental aerodynamic loads and provides additional insight into flow structures, pressure distributions and component-level force contributions. This enables analysis of operating scenarios beyond the scope of wind-tunnel testing, including high-speed headwinds and multi-pantograph configurations. The simulations reveal significant aerodynamic interference effects between pantographs, influenced by spacing, roof-flow development and knuckle orientation.

Results demonstrate that knuckle orientation strongly affects the total uplift force applied on the OLE contact wire, mainly due to the angle of the pantograph vanes. This highlights the need for optimisation and correct pantograph setup to achieve stable contact quality in both train travel directions. Dynamic simulations show that aerodynamic loads can increase contact force levels and variability, but these generally remain within acceptable limits. Overall, the study establishes a validated methodology for evaluating wind-induced pantograph performance and provides guidance for improving pantograph-OLE interaction, its analysis via dynamic simulation, operational strategies and future industry standards.

Acknowledgements

This work was financially supported by Network Rail, UK.

References

[1] EN 50317:2025. Railway applications - Current collection systems - Requirements for and validation of measurements of the dynamic interaction between pantograph and overhead contact line. 2025.

[2] EN 50318:2018+A1:2022. Railway applications - Current collection systems - Validation of simulation of the dynamic interaction between pantograph and overhead contact line 2022.

[3] EN 50367:2020. Railway Applications - Current Collection Systems - Technical Criteria for the Interaction Between Pantograph and Overhead Line 2020.

[4] Ambrósio J, Pombo J, Antunes P, Pereira M. PantoCat statement of method. Vehicle System Dynamics 2015;53:314–28. https://doi.org/10.1080/00423114.2014.969283.

[5] Antunes P, Ambrósio J, Pombo J, Facchinetti A. A new methodology to study the pantograph–catenary dynamics in curved railway tracks. Vehicle System Dynamics 2020;58:425–52. https://doi.org/10.1080/00423114.2019.1583348.

[6] Pombo J, Antunes P, Rebelo J. PantoCat Certification, D1.2: Conformance of PantoCat with EN50318:2018 for the 'AC Simple' Catenary. Institute of Railway Research, University of Huddersfield, UK: 2020.

[7] Pombo J, Antunes P, Rebelo J. PantoCat Certification, D1.1: Conformance between PantoCat and the Certified Tools PCaDA (POLIMI) and OSCAR (SNCF). Institute of Railway Research, University of Huddersfield, UK: 2020.

[8] NCB. Design Examination Type Certificate for PantoCat (version 5.1). Network Certification Body, Certificate Number: NCB_N04901_Cert_4085, UK: 2020.

[9] Pombo J, Ambrósio J, Pereira M, Rauter F, Collina A, Facchinetti A. Influence of the aerodynamic forces on the pantograph–catenary system for

high-speed trains. Vehicle System Dynamics 2009;47:1327–47. https://doi.org/10.1080/00423110802613402.

[10] Jackson FF, Mishra R, Rebelo JM, Santos J, Antunes P, Pombo J, et al. Modelling dynamic pantograph loads with combined numerical analysis. Railway Engineering Science 2024;32:81–94. https://doi.org/10.1007/s40534-023-00318-0.

[11] Network Rail. UKMS System Description Manual Issue 2.2 (ref. 141667-FAF-MAN-EOH-000001). 2022.

[12] EN 50318:2018. Railway Applications - Current Collection Systems - Validation of Simulation of the Dynamic Interaction Between Pantograph and Overhead Contact Line 2018.

[13] RSSB. Lump mass models for legacy pantographs on GB mainline. 2016.

[14] Brecknell Willis. BW14437 - Dynamic Testing of the HSP, HSP Mk2 and HSX Pantographs on the DB Munich Test Bench - Revision 02. 2012.